AGU PUBLICATIONS

Geophysical Research Letters

RESEARCH LETTER
10.1002/2016GL070170

Key Points:
- We simulate subglacial plumes and submarine melt in 12 Greenland fjords spanning grounding line depths from 100 to 850 m
- Deep glaciers produce warm, salty subsurface plumes that undercut ice; shallow glaciers drive cold, fresh surface plumes that can overcut
- Plumes in cold, shallow fjords can induce comparable depth-averaged melt rates to warm, deep fjords due to sustained upwelling velocities

Supporting Information:
- Supporting Information S1

Correspondence to:
D. Carroll,
dcarroll@uoregon.edu

Citation:
Carroll, D., et al. (2016), The impact of glacier geometry on meltwater plume structure and submarine melt in Greenland fjords, *Geophys. Res. Lett.*, *43*, 9739–9748, doi:10.1002/2016GL070170.

Received 23 JUN 2016
Accepted 9 SEP 2016
Accepted article online 10 SEP 2016
Published online 29 SEP 2016

The impact of glacier geometry on meltwater plume structure and submarine melt in Greenland fjords

D. Carroll[1], D. A. Sutherland[1], B. Hudson[2], T. Moon[1,3], G. A. Catania[4,5], E. L. Shroyer[6], J. D. Nash[6], T. C. Bartholomaus[4,5], D. Felikson[4,5], L. A. Stearns[7], B. P. Y. Noël[8], and M. R. van den Broeke[8]

[1]Department of Earth Sciences, University of Oregon, Eugene, Oregon, USA, [2]Applied Physics Laboratory, University of Washington, Seattle, Washington, USA, [3]Bristol Glaciology Centre, School of Geographical Sciences, University of Bristol, Bristol, UK, [4]Institute for Geophysics, University of Texas, Austin, Texas, USA, [5]Department of Geology, University of Texas, Austin, Texas, USA, [6]College of Earth, Ocean, and Atmospheric Sciences, Oregon State University, Corvallis, Oregon, USA, [7]Department of Geology, University of Kansas, Lawrence, Kansas, USA, [8]Institute for Marine and Atmospheric Research Utrecht, Utrecht University, Utrecht, Netherlands

Abstract Meltwater from the Greenland Ice Sheet often drains subglacially into fjords, driving upwelling plumes at glacier termini. Ocean models and observations of submarine termini suggest that plumes enhance melt and undercutting, leading to calving and potential glacier destabilization. Here we systematically evaluate how simulated plume structure and submarine melt during summer months depends on realistic ranges of subglacial discharge, glacier depth, and ocean stratification from 12 Greenland fjords. Our results show that grounding line depth is a strong control on plume-induced submarine melt: deep glaciers produce warm, salty subsurface plumes that undercut termini, and shallow glaciers produce cold, fresh surface-trapped plumes that can overcut termini. Due to sustained upwelling velocities, plumes in cold, shallow fjords can induce equivalent depth-averaged melt rates compared to warm, deep fjords. These results detail a direct ocean-ice feedback that can affect the Greenland Ice Sheet.

1. Introduction

Mass loss from the Greenland Ice Sheet quadrupled from 1992 to 2011 [*Shepherd et al.*, 2012]. The acceleration, retreat, and thinning of outlet glaciers [*van den Broeke et al.*, 2009; *Enderlin et al.*, 2014] coincided with a warming of Atlantic waters [*Straneo and Heimbach*, 2013], leading to the hypothesis that marine-terminating glaciers are sensitive to ocean forcing [*Vieli and Nick*, 2011]. On the Greenland shelf, warm, salty Atlantic water is typically found at depth, overlaid by cold, fresh Polar water and a seasonal layer of warm surface water [*Straneo et al.*, 2012]. Warming of subsurface Atlantic waters in Greenland fjords can lead to increased submarine melting [*Holland et al.*, 2008; *Motyka et al.*, 2011], which has been implicated as a mechanism for promoting calving [*O'Leary and Christoffersen*, 2013; *Luckman et al.*, 2015] and accelerating glacier flow [*Nick et al.*, 2009].

Submarine melting is determined by the net ocean heat flux to the ocean-ice boundary layer through processes that are highly dependent on fjord circulation [*Straneo et al.*, 2010, 2011, 2012]. Previous work shows that there is large regional and temporal variability in fjord circulation. For example, southeast Greenland fjords are forced by subglacial plumes during summer [*Straneo et al.*, 2011] and dominated by shelf-forced flows during winter [*Jackson et al.*, 2014; *Jackson and Straneo*, 2016]. Subglacial plumes are a primary feature of west Greenland fjords during summer [*Mortensen et al.*, 2013; *Chauché et al.*, 2014; *Bartholomaus et al.*, 2016] and may be relatively more important year-round compared to southeast Greenland due to the lack of strong shelf-forced flows. Given uncertainty in the relative importance of shelf-forced circulation across Greenland, it is first necessary to characterize subglacial plumes—the most commonly observed feature thought to be dominantly responsible for terminus melt and fjord circulation during the meltwater season [*Straneo and Cenedese*, 2015].

Our understanding of how subglacial plumes vary across Greenland fjords is, however, severely limited. Direct observations of plumes are sparse due to the difficult working conditions at calving termini [*Stevens et al.*, 2016]. Recent work tracing the pathways of glacially modified water suggests heterogeneity in plume properties, with shallow glaciers unable to entrain deep reservoirs of Atlantic-origin water [*Beaird et al.*, 2015].

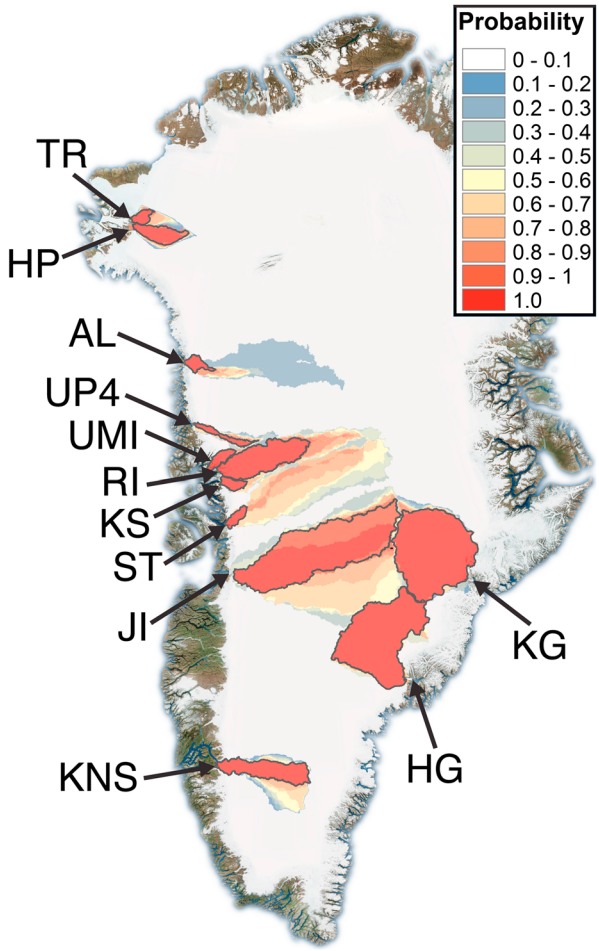

Figure 1. Greenland outlet glaciers examined in this study and their respective probability-based catchments. The colors show the probability that a region of the ice sheet contributes meltwater to the outlet glacier; the grey boundaries represent the 95% probability level catchments used to estimate subglacial discharge.

Previous theoretical results [*Jenkins*, 2011; *Slater et al.*, 2016] and numerical ocean models [*Xu et al.*, 2012, 2013; *Sciascia et al.*, 2013; *Cowton et al.*, 2015; *Slater et al.*, 2015; *Carroll et al.*, 2015] have provided key insight into plume dynamics at glacier termini. However, no systematic set of sensitivity experiments has been conducted to show how subglacial plumes and submarine melt rates in Greenland fjords vary over the broad range of observed oceanographic stratification profiles, with all of the environmental complexities that this entails.

Here we use a buoyant plume model [*Cowton et al.*, 2015] paired with shipboard hydrographic observations to characterize subglacial plumes and submarine melt in 12 major Greenland fjords (Figure 1 and Table 1). We show that systematic differences in modeled plume circulation at mean summer discharge levels are due to variability in grounding line depth and fjord hydrography, demonstrating that the coupled fjord-glacier system is responsible for modulating the mixing of ice sheet runoff with seawater. While our analysis is limited to fjords with available hydrographic and bathymetric data, our study encompasses

Table 1. Mean Grounding Line Depth (GL), Mean Depth-Averaged Ocean Temperature (Ocean *T*), Mean Ocean Heat Content (OHC), and Summer Hydrographic Data Coverage for All Modeled Systems[a]

Glacier	GL (m)	Ocean *T* (°C)	OHC (GJ m^{-2})	Hydrographic Data
Upernavik 4 (UP4)	100	1.35 ± 0.11	1.68 ± 0.07	2013[b] and 2015
Umiamako (UMI)	230	1.56 ± 0.01	3.38 ± 0.05	2013
Kangerdlugssup Sermerssua (KS)	250	1.12 ± 0.16	2.86 ± 0.13	2013–2015
Kangiata Nunata Sermia (KNS)	250	1.80 ± 0.45	3.85 ± 0.65	2006, 2007[b]–2009, and 2011–2013
Heilprin (HP)	350	0.64 ± 0.01	2.03 ± 0.15	2003
Store (ST)	500	2.07	7.19	2010[b]
Tracy (TR)	610	0.73 ± 0.01	3.85 ± 0.21	2003
Helheim (HG)	650	2.70 ± 0.44	15.3 ± 2.29	2008–2012
Kangerdlugssuaq (KG)	650	0.80 ± 0.18	5.07 ± 0.68	1993, 2004, 2009, and 2012
Jakobshavn (JI)	800	2.43 ± 0.01	17.1 ± 0.11	2009
Alison (AL)	850	1.17	9.34	2014[b]
Rink Isbræ (RI)	850	2.32 ± 0.07	16.5 ± 0.74	2013–2015

[a]The errors in ocean temperature and heat content represent the uncertainty (1 standard deviation) due to temporal and spatial variability in fjord stratification. Supporting information contains additional details on grounding line depth and hydrographic data sources.
[b]Single CTD cast is denoted.

a greater range of observed summer ocean properties and grounding line depths than previously examined (Tables 1 and S1 in the supporting information) [*Straneo et al*., 2012]. We generate daily estimates of subglacial discharge for each glacier by pairing a probability-based algorithm for delineating ice sheet catchments with a high-resolution model of surface runoff [*Noël et al*., 2015]. Finally, we utilize repeated hydrographic surveys to show that our results are robust to synoptic and interannual variability in fjord stratification.

2. Materials and Methods

2.1. Subglacial Plume Model

We use a steady state plume model to characterize subglacial plumes rising along a melting, vertical terminus. The governing equations are based on a stream tube model [*Smith*, 1975; *Killworth*, 1977; *MacAyeal*, 1985; *Jenkins*, 2011], modified for a half-conical plume forced by a discrete source of subglacial discharge [*Cowton et al*., 2015, equations (1)–(4)]. The entrainment rate of ocean water into the plume (u_e) is parameterized as

$$u_e = \alpha w,$$

where α is equal to 0.1 [*Morton et al*., 1956] and w is the vertical velocity of the plume. All plume properties have a uniform top-hat profile along the cross section of the plume. We define the terminal level as the depth where the plume reaches neutral buoyancy and intrudes horizontally into the fjord, consistent with results from high-resolution ocean models [*Cowton et al*., 2015; *Carroll et al*., 2015]. Following *Cowton et al*. [2015], the initial velocity of the plume (w_0) is fixed to 1 m s^{-1} and the initial plume radius (r_0) is given by

$$r_0 = \sqrt{\frac{2Q_{sg}}{\pi w_0}},$$

where Q_{sg} is the initial subglacial discharge flux. The initial plume temperature and salinity are set to the pressure-dependent melting point and 0, respectively. As the plume rises along the terminus, its volume increases due to entrainment of fjord waters and submarine melt. We calculate the plume dilution (D_{plume}), the ratio of vertical flux across a semicircular plume cross section of radius r compared to the initial subglacial discharge, as

$$D_{plume}(z) = \frac{\pi r(z)^2 w(z)}{2Q_{sg}},$$

where z is the depth and w is the vertical velocity of the plume.

2.2. Submarine Melt Rate

To estimate the submarine melt of ice from the subglacial plume, we solve a three-equation model [*Holland and Jenkins*, 1999] describing conservation of heat and salt at the ocean-ice boundary, combined with a liquidus constraint at the interface:

$$\dot{m}(c_i(T_b - T_{ice}) + L) = \Gamma_T C_d^{1/2} c_p w(T_{plume} - T_b),$$
$$\dot{m}S_b = \Gamma_s C_d^{1/2} w(S_{plume} - S_b),$$
$$T_b = \lambda_1 S_b + \lambda_2 + \lambda_3 z,$$

where $\dot{m}$ is the melt rate, L is the latent heat of fusion, c_i and c_p are the specific heat capacities of ice and water, T_b and T_{ice} are the ocean-ice boundary and ice temperature, S_b and S_{plume} are the ocean-ice boundary and plume salinity, ${C_d}^{1/2}\Gamma_T$ and ${C_d}^{1/2}\Gamma_S$ are the thermal and haline Stanton numbers, λ_{1-3} are the constants that describe the dependence of freezing point on salinity and pressure, and z is the depth. All parameters follow values given in *Jenkins* [2011]. We note that the plume model does not capture the potential inertial rebound of the plume to the level of neutral buoyancy [*Morton et al*., 1956; *Carroll et al*., 2015]; this flow may contribute to additional melt above the terminal level.

2.3. Fjord Hydrography

We use a compilation of shipboard surveys across Greenland fjords to provide temperature and salinity boundary conditions for the subglacial plume model (Tables 1 and S1). All profiles are depth averaged into

2 m bins. We assume that each survey is representative of typical hydrographic conditions during the summer. Systems with hydrographic profiles that do not extend to the grounding line depth are extrapolated assuming constant values below the depth of measurements. We calculate ocean heat content (OHC) as

$$\mathrm{OHC} = \int_{-gl}^{0} \rho_0 c_p T \, dz,$$

where *gl* is the grounding line depth, ρ_0 is a reference density, and T is the ocean temperature.

2.4. Subglacial Discharge

To estimate subglacial discharge we integrate daily surface runoff from the Regional Atmospheric Climate Model version 2.3 downscaled to 1 km using elevation dependence (version 0.2) over each outlet glacier catchment [*Noël et al*., 2015]. We assume that all surface runoff drains immediately to the glacier bed, with no water storage. To create probability-based catchments, we apply a Monte Carlo-based approach to calculate each outlet's catchment over a range of bed topographic maps varied within published error ranges. We randomly vary the bed topography [*Morlighem et al*., 2015] by multiplying the published error range by a random, uniformly distributed number between −1 and 1 and add it to the published bed topography. For each iteration of the bed topography, we then calculate the hydraulic potentiometric surface, φ, using basal topography, z_{bed}, and ice surface topography data, z_{ice} [*Morlighem et al*., 2014]. Following the standard procedure of *Lewis and Smith* [2009] and *Cuffey and Paterson* [2010], we calculate φ as

$$\varphi = \rho_{\mathrm{ice}} g \left(z_{\mathrm{ice}} + \frac{(\rho_w - \rho_i)}{\rho_i} z_{\mathrm{bed}} \right),$$

where ρ_{ice} is the density of ice, ρ_w is the density of freshwater, and g is the acceleration due to gravity. Next we determine the flow path of water along this hydraulic potentiometric surface using a simple D8 approach implemented in the TauDEM C++ software package [*Tarboton*, 1997]. The D8 method assigns flow from each pixel to one of its eight neighbors (adjacent or diagonal) in the direction of steepest downslope [*O'Callaghan and Mark*, 1984]. We then use Environmental Systems Research Institute's ArcPy Basin function to delineate catchments from the D8 direction grid. This algorithm starts at a given outlet location and recursively searches upstream from the outlet for cells that contributed to it. We flag all cells found by this recursive search as within the hydrologic catchment. After all iterations of catchment boundaries are found, we sum the number of times the pixel was in the catchment, x, and divide it by the number of times the bed was varied, n.

$$\text{For pixel } (i,j) = \frac{(\Sigma\, x(i,j))}{n(i,j)}.$$

This provides the per outlet probability that a part of the ice sheet contributes runoff to it. We use the 95% probability area as the catchment boundary for all outlet glacier systems in this study.

3. Results

We first examine the sensitivity of all systems to variability in subglacial discharge and fjord hydrography (Figure 2). Shallow systems (defined as grounding line depth ≤500 m) produce plumes with terminal levels (depth where plume intrudes horizontally into the fjord) that are confined to the upper 100 m during mean summer discharge levels, becoming surface trapped at peak discharge (Figure 2a). In deeper systems (>500 m), plumes are unable to penetrate into the buoyant surface water layer, resulting in deep, subsurface plumes (100–250 m depth). Regional variability in ocean heat content at depth drives marked differences in plume melt rate. For example, mean plume melt rate is 93% larger in Helheim (HG) than Kangerdlugssuaq (KG) despite similar grounding line depths (Figure 2b).

For adjacent fjords exposed to similar hydrographic properties, such as Kangerdlugssup Sermerssua (KS) and Rink Isbræ (RI), increasing the grounding line depth (250 versus 850 m) results in a deepening of the mean plume terminal level from 25 to 223 m, respectively, and a 45% increase in mean plume melt rate. Increasing subglacial discharge in shallow systems (grounding line depth ≤500) generally produces plumes with progressively larger negative temperature and salinity anomalies; i.e., plumes become colder and

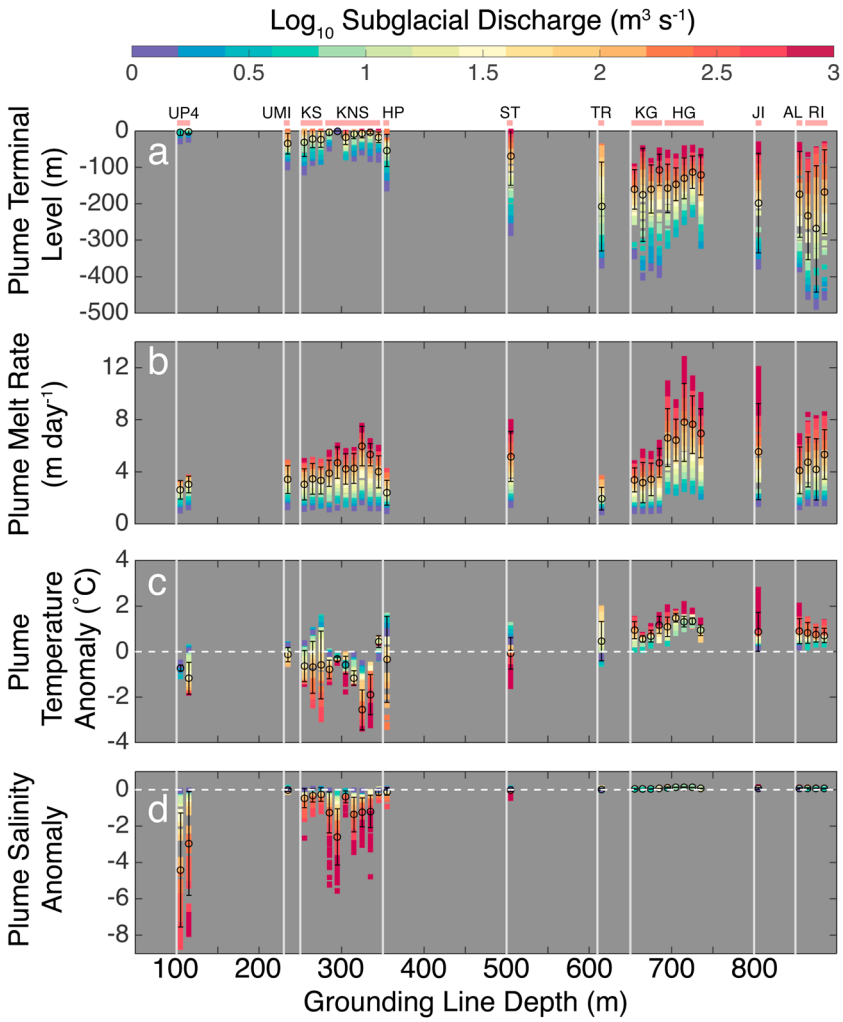

Figure 2. Subglacial plume properties for all 12 fjord-glacier systems. (a) Sensitivity of plume terminal level, (b) depth-averaged melt rate, (c) temperature anomaly, and (d) salinity anomaly to subglacial discharge. The vertical lines represent the grounding line depths for the glaciers examined in this study. The vertical bars to the right of the each line show the plume properties in chronological order for each glacier with that grounding line depth. The vertical bars are spaced at 10 m intervals for visibility; the colors show the rate of subglacial discharge. The circles are the mean summer values, and the error bars represent the uncertainty (1 standard deviation) due to temporal variability in subglacial discharge. Hydrographic profiles are averaged across each summer. Plume temperature and salinity anomaly are taken with respect to ambient fjord waters at the terminal level; salinity is expressed in Practical Salinity Scale.

fresher as discharge increases (Figures 2c and 2d and S1 in the supporting information). Increasing subglacial discharge in deeper systems results in plumes with positive temperature and salinity anomalies that equilibrate within the Polar water layer.

For fixed subglacial discharge, plume melt rate depends on ocean heat content and grounding line depth, with grounding line depth providing a first-order control on how efficiently the plume can transfer ocean heat to the ice to allow for melting (Figure 3a). All systems collapse into characteristic lines based on their grounding line depth; synoptic and interannual variability in ocean heat content determine the plume melt rate along each line. The depth-dependent grouping of the systems is robust for a range of selected subglacial discharges (50–500 $m^3 s^{-1}$); larger discharges result in steeper slopes due to increased plume melt rate (Table S3). Shallow systems (G1 and G2) have steeper slopes (larger depth-averaged melt rate change per ocean heat content) because surface-reaching plumes retain large velocities along the entire terminus (Figure S2). For equivalent ocean heat content, deeper systems (G3 and G4) have shallower slopes due to dilution of the plume at depth by entrainment, resulting in weaker depth-averaged plume velocities.

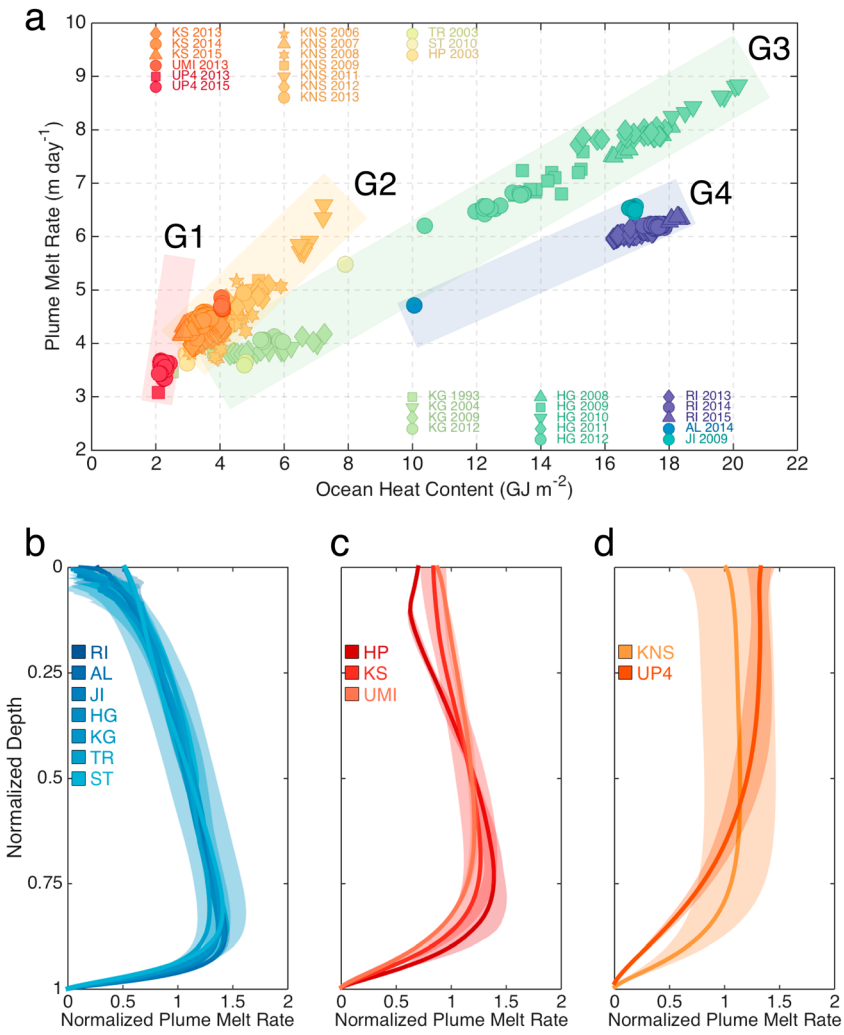

Figure 3. Sensitivity of plume melt rate to ocean heat content and corresponding vertical structure. Subglacial discharge is fixed at 250 $m^3 s^{-1}$; all available profiles for each system are used. (a) Sensitivity of depth-averaged plume melt rate to ocean heat content. All systems collapse along characteristic lines due to their grounding line depth (G_1 = 100 m, G_2 = 230–250 m, G_3 = 650 m, and G_4 = 800–850 m). Profiles of plume melt rate for all systems, with (b) undercut (500–850 m), (c) semiuniform (230–350 m), and (d) overcut (100–250 m) melt distribution. Plume melt rate and depth are normalized by their depth-averaged and maximum values, respectively. The shaded error bars represent the uncertainty (2 standard deviations) due to spatial and temporal variability in fjord stratification.

Increasing the grounding line depth from 100 to 850 m (UP4 versus RI) results in a 30% decrease in depth-averaged plume vertical velocity. Additionally, shallow and deep systems (such as Kangiata Nunata Sermia and KG, respectively) can have equivalent depth-averaged plume melt rates due to the dependence of submarine melt on both vertical velocity and temperature.

Grounding line depth strongly modulates the vertical distribution of submarine melt (Figures 3b–3d and S3). In deep systems (500–850 m grounding line depth), the subglacial plume is rapidly decelerated by entrainment of warm Atlantic water at depth, increasing the plume temperature and leading to maximum melt rates in the lower water column, suggestive of glacial undercutting (Figure 3b). Directly above the grounding line, the plume consists of relatively undiluted, cold subglacial discharge—resulting in a region of low melt and indicative of a protruding ice "toe." As the grounding line depth is decreased (230–350 m), plumes entrain a larger percentage of cold Polar water, resulting in semiuniform melt profiles with maxima higher in the water column (Figure 3c). Systems with shallow grounding lines (100–250 m) and warm surface water temperatures result in overcut melt profiles with maxima in the upper half of the water column (Figure 3d).

For low subglacial discharge ($\leq$50 $m^3 s^{-1}$), shallow systems relax toward undercut melt profiles (as shown in Figure 3b), as weakly buoyant plumes reach their terminal level at greater depth.

4. Discussion

Our results emphasize the important connection between the terrestrial ice sheet runoff signal and plume-induced circulation. Given basic observations, our results provide first-order rules of thumb for estimating the impact of plume melting on a glacier terminus. As new bathymetric and hydrographic observations become available, we anticipate that this study will aid in predictions of plume properties across Greenland fjords. Based on a realistic range of subglacial discharge, grounding line depth, and ocean heat content, we have several critical findings: (i) grounding line depth and large-scale regional changes in ocean heat content exert a strong control on subglacial plumes; (ii) cold, fast plumes in shallow systems and warm, slow plumes in deep systems can induce equivalent localized depth-averaged melt rates; and (iii) deeply grounded glaciers result in undercut termini, and shallow glaciers support semiuniform or overcut termini.

These two glacier geometries (deep versus shallow) produce marked differences in fjord temperature and salinity at the plume terminal level, present across a variety of subglacial discharge rates and conduit configurations (Figure S4). Our results exhibit similar qualitative trends to the scalings obtained by *Slater et al*. [2016]; however, future work is needed to determine if these scalings hold quantitatively for the realistic stratification observed in Greenland fjords. This study, consistent with observations and idealized ocean models [*Straneo et al*., 2011; *Xu et al*., 2012, 2013; *Sciascia et al*., 2013; *Carroll et al*., 2015], demonstrates that deep fjords act as subsurface pathways for mixing and export of ice sheet runoff. These results call into question surface-injected parameterizations of runoff in current climate models, where the vertical ocean grid resolution is sufficiently fine to incorporate subsurface runoff fluxes [*Lenaerts et al*., 2015]. Additionally, the increase of plume dilution with grounding line depth suggests that deep systems drive more vigorous depth-integrated exchange within the fjord, implying faster replenishment of fjord waters (Figure S5).

Our results suggest that regions near subglacial conduits can support a variety of terminus geometries, potentially leading to a complex calving front evolution during the meltwater season. Recent observations of the KS terminus add support to this hypothesis, showing a diverse spatial distribution of undercut and overcut regions [*Fried et al*., 2015]. We acknowledge that our model does not couple the ice front profile and plume, which may neglect important plume-ice feedbacks. In regions where the terminus becomes overcut or near a protruding ice toe, the plume may detach—decreasing melt rates and the level of overcutting until the plume regains contact with the ice. The plume model results in localized melt rates on the order of meters per day, in general agreement with direct observations [*Fried et al*., 2015] and bulk estimates based on conservation of heat, salt, and mass [*Rignot et al*., 2010; *Sutherland and Straneo*, 2012; *Xu et al*., 2013]. However, our estimated melt rates are limited to a localized area (~100 m wide) on either side of the plume. Spatially averaging melt across the terminus from a single plume results in melt rates biased ~2 orders of magnitude low compared to observations (2.0 m d^{-1} observed for KS; Text S1 and Figure S6 in the supporting information) [*Fried et al*., 2015]. These results imply that while a single plume may induce significant localized submarine melt, a distributed subglacial drainage system may be needed to influence calving and produce terminus retreat driven by undercutting [*Slater et al*., 2015; *Rignot et al*., 2016b]. We stress that our parameterized melt rates are sensitive to the choice of turbulent transfer coefficients, developed for sloping ice shelves [*Holland and Jenkins*, 1999; *Jenkins et al*., 2010] and yet to be validated for Greenland's near vertical termini [*Rignot et al*., 2015; *Fried et al*., 2015]. Ultimately, coincident ocean and terminus ablation measurements are needed to constrain turbulent transfer coefficients and determine if submarine melt can exceed typical calving rates observed at large marine-terminating glaciers in Greenland.

To guide future observational programs, we find that plume melt rate is generally insensitive to the distance hydrographic measurements are made from the glacier (largest relative change from near glacier to mouth was 16% for HG), as long as observations are made near the fjord where variability in ambient temperature is small and not on the shelf (Figure S7). However, plume terminal level is more sensitive to measurement location, deepening by 31% in RI when using profiles from the mouth compared to near glacier, due to stronger stratification downfjord. For fjords with shallow sills, we would expect large variability in stratification landward and seaward of the sill, suggesting that near-glacier measurements may be necessary in systems with isolated basins.

We note that our results only apply to subglacial plume dynamics at the terminus. We have neglected potentially important external forcing such as wind, tides, and shelf-forced circulation [*Straneo et al*., 2010; *Mortensen et al*., 2013; *Jackson et al*., 2014]. While we anticipate the interaction of plume- and externally-forced circulation to drive variability in fjord stratification and heat content, the exchange of heat and salt at the ocean-ice boundary will be largely dominated by subglacial plumes during the meltwater season because these are what drive the deep, net flows toward the glacier.

5. Conclusion

We have produced the first systematic characterization of subglacial plumes in Greenland outlet glacier fjords with grounding line depths that range from 100 to 850 m. We propose that subglacial plumes can drive substantial localized terminus melt, representing an important ocean-ice feedback that strongly depends on glacier geometry and can affect the ice sheet mass balance. This work stresses the need for realistic termini morphology in high-resolution ocean models and subsurface parameterizations of ice sheet runoff in large-scale climate models. Ultimately, a detailed understanding of plume-glacier interactions allows for improved constraints on sea level rise from the Greenland Ice Sheet.

Acknowledgments
This work was partially supported by the National Aeronautics and Space Administration grant NNX12AP50G and the University of Oregon. M.R. van den Broeke and B.P.Y. Noël acknowledge financial support from the Polar Program of the Netherlands Organization for Scientific Research (NWO) and the Netherlands Earth System Science Center. T. Moon acknowledges support from the NSF OCE Postdoctoral Fellowship. We thank two anonymous reviewers for their thoughtful and constructive criticism of this work. Data used in this work are available by e-mailing the corresponding author.

References

Andresen, C. S., K. K. Kjeldsen, B. Harden, N. Nørgaard-Pedersen, and K. H. Kjær (2014), Outlet glacier dynamics and bathymetry at Upernavik Isstrøm and Upernavik Isfjord north-west Greenland, *Geol. Surv. Den. Greenl. Bull.*, *31*, 79–82.

Azetsu-Scott, K., and F. C. Tan (1997), Oxygen isotope studies from Iceland to an east Greenland fjord: Behaviour of glacial meltwater plume, *Mar. Chem.*, *56*(3), 239–251.

Bartholomaus, T. C., et al. (2016), Contrasts in the response of adjacent fjords and glaciers to surface melt in western Greenland, *Ann. Glaciol.*, 1–14, doi:10.1017/aog.2016.19.

Beaird, N., F. Straneo, and W. Jenkins (2015), Spreading of Greenland meltwaters in the ocean revealed by noble gases, *Geophys. Res. Lett.*, *42*, 7705–7713, doi:10.1002/2015GL065003.

Bendtsen, J., J. Mortensen, K. Lennert, and S. Rysgaard (2015), Heat sources for glacial ice melt in a west Greenland tidewater outlet glacier fjord: The role of subglacial freshwater discharge, *Geophys. Res. Lett.*, *42*, 4089–4095, doi:10.1002/2015GL063846.

Boghosian, A., K. Tinto, J. R. Cochran, D. Porter, S. Elieff, B. L. Burton, and R. E. Bell (2015), Resolving bathymetry from airborne gravity along Greenland fjords, *J. Geophys. Res. Solid Earth*, *120*, 8516–8533, doi:10.1002/2015JB012129.

Carroll, D., D. A. Sutherland, E. L. Shroyer, J. D. Nash, G. A. Catania, and L. A. Stearns (2015), Modeling turbulent subglacial meltwater plumes: Implications for fjord-scale buoyancy-driven circulation, *J. Phys. Oceanogr.*, *45*(8), 2169–2185.

Chauché, N., A. Hubbard, J. C. Gascard, J. E. Box, R. Bates, M. Koppes, and H. Patton (2014), Ice–ocean interaction and calving front morphology at two west Greenland tidewater outlet glaciers, *Cryosphere*, *8*(4), 1457–1468.

Christoffersen, P., R. I. Mugford, K. J. Heywood, I. Joughin, J. A. Dowdeswell, J. P. M. Syvitski, and T. J. Benham (2011), Warming of waters in an east Greenland fjord prior to glacier retreat: Mechanisms and connection to large-scale atmospheric conditions, *Cryosphere*, *5*(3), 701–714.

Cofaigh, C. Ó., J. A. Dowdeswell, A. E. Jennings, K. A. Hogan, A. Kilfeather, J. F. Hiemstra, and J. M. Lloyd (2013), An extensive and dynamic ice sheet on the west Greenland shelf during the last glacial cycle, *Geology*, *41*(2), 219–222.

Cowton, T., D. Slater, A. Sole, D. Goldberg, and P. Nienow (2015), Modeling the impact of glacial runoff on fjord circulation and submarine melt rate using a new subgrid-scale parameterization for glacial plumes, *J. Geophys. Res. Oceans*, *120*, 796–812, doi:10.1002/2014JC010324.

Cuffey, K. M., and W. S. B. Paterson (2010), *The Physics of Glaciers*, Academic Press, Cambridge, Mass.

Dowdeswell, J. A., K. A. Hogan, C. Ó. Cofaigh, E. M. G. Fugelli, J. Evans, and R. Noormets (2014), Late Quaternary ice flow in a west Greenland fjord and cross-shelf trough system: Submarine landforms from Rink Isbrae to Uummannaq shelf and slope, *Quat. Sci. Rev.*, *92*, 292–309.

Enderlin, E. M., I. M. Howat, S. Jeong, M. J. Noh, J. H. Angelen, and M. R. Broeke (2014), An improved mass budget for the Greenland Ice Sheet, *Geophys. Res. Lett.*, *41*, 866–872, doi:10.1002/2013GL059010.

Fried, M. J., G. A. Catania, T. C. Bartholomaus, D. Duncan, M. Davis, L. A. Stearns, and D. A. Sutherland (2015), Distributed subglacial discharge drives significant submarine melt at a Greenland tidewater glacier, *Geophys. Res. Lett.*, *42*, 9328–9336, doi:10.1002/2015GL065806.

Gladish, C. V., D. M. Holland, A. Rosing-Asvid, J. W. Behrens, and J. Boje (2015), Oceanic boundary conditions for Jakobshavn glacier. Part I: Variability and renewal of Ilulissat Icefjord waters, 2001–14*, *J. Phys. Oceanogr.*, *45*(1), 3–32.

Holland, D. M., and A. Jenkins (1999), Modeling thermodynamic ice-ocean interactions at the base of an ice shelf, *J. Phys. Oceanogr.*, *29*(8), 1787–1800.

Holland, D. M., R. H. Thomas, B. De Young, M. H. Ribergaard, and B. Lyberth (2008), Acceleration of Jakobshavn Isbrae triggered by warm subsurface ocean waters, *Nat. Geosci.*, *1*(10), 659–664.

Inall, M. E., T. Murray, F. R. Cottier, K. Scharrer, T. J. Boyd, K. J. Heywood, and S. L. Bevan (2014), Oceanic heat delivery via Kangerdlugssuaq Fjord to the south-east Greenland Ice Sheet, *J. Geophys. Res. Oceans*, *119*, 631–645, doi:10.1002/2013JC009295.

Jackson, R., and F. Straneo (2016), Heat, salt, and freshwater budgets for a glacial fjord in Greenland, *J. Phys. Oceanogr.*, doi:10.1175/JPO-D-15-0134.1, in press.

Jackson, R. H., F. Straneo, and D. A. Sutherland (2014), Externally forced fluctuations in ocean temperature at Greenland glaciers in non-summer months, *Nat. Geosci.*, *7*(7), 503–508.

Jenkins, A. (2011), Convection-driven melting near the grounding lines of ice shelves and tidewater glaciers, *J. Phys. Oceanogr.*, *41*(12), 2279–2294.

Jenkins, A., K. W. Nicholls, and H. F. Corr (2010), Observation and parameterization of ablation at the base of Ronne Ice Shelf, Antarctica, *J. Phys. Oceanogr.*, *40*(10), 2298–2312.

Joughin, I., and T. Moon (2015), *MEaSUREs Annual Greenland Outlet Glacier Terminus Positions from SAR Mosaics [73°N, 72°W; 63°N, 32°W]*, NASA National Snow and Ice Data Center Distributed Active Archive Center, Boulder, Colo., doi:10.5067/DC0MLBOCL3EL, Accessed October 18, 2015.

Killworth, P. D. (1977), Mixing of the Weddell Sea continental slope, *Deep Sea Res.*, *24*(5), 427–448.

Lenaerts, J., D. Le Bars, L. Kampenhout, M. Vizcaino, E. M. Enderlin, and M. R. Broeke (2015), Representing Greenland Ice Sheet freshwater fluxes in climate models, *Geophys. Res. Lett.*, *42*, 6373–6381, doi:10.1002/2015GL064738.

Lewis, S. M., and L. C. Smith (2009), Hydrologic drainage of the Greenland Ice Sheet, *Hydrol. Processes*, *23*(14), 2004.

Luckman, A., D. I. Benn, F. Cottier, S. Bevan, F. Nilsen, and M. Inall (2015), Calving rates at tidewater glaciers vary strongly with ocean temperature, *Nat. Commun.*, *6*.

MacAyeal, D. R. (1985), Evolution of tidally triggered meltwater plumes below ice shelves, *Oceanol. Antarct. Cont. Shelf*, 133–143.

Moon, T., and I. Joughin (2008), Changes in ice front position on Greenland's outlet glaciers from 1992 to 2007, *J. Geophys. Res.*, *113*, F02022, doi:10.1029/2007JF000927.

Moon, T., I. Joughin, B. Smith, M. R. Broeke, W. J. Berg, B. Noël, and M. Usher (2014), Distinct patterns of seasonal Greenland glacier velocity, *Geophys. Res. Lett.*, *41*, 7209–7216, doi:10.1002/2014GL061836.

Morlighem, M., E. Rignot, J. Mouginot, H. Seroussi, and E. Larour (2014), Deeply incised submarine glacial valleys beneath the Greenland Ice Sheet, *Nat. Geosci.*, *7*(6).

Morlighem, M., E. Rignot, J. Mouginot, H. Seroussi and E. Larour (2015), *IceBridge BedMachine Greenland, Version 2 [73°N, 72°W; 63°N, 32°W]*, NASA DAAC at the National Snow and Ice Data Center, Boulder, Colo., doi:10.5067/AD7B0HQNSJ29.

Mortensen, J., J. Bendtsen, R. J. Motyka, K. Lennert, M. Truffer, M. Fahnestock, and S. Rysgaard (2013), On the seasonal freshwater stratification in the proximity of fast-flowing tidewater outlet glaciers in a sub-Arctic sill fjord, *J. Geophys. Res. Oceans*, *118*, 1382–1395, doi:10.1002/jgrc.20134.

Morton, B. R., G. Taylor, and J. S. Turner (1956), Turbulent gravitational convection from maintained and instantaneous sources, *Proc. R. Soc. Lond. A: Math. Phys. Eng. Sci.*, *234*(1196), 1–23.

Motyka, R. J., M. Truffer, M. Fahnestock, J. Mortensen, S. Rysgaard, and I. Howat (2011), Submarine melting of the 1985 Jakobshavn Isbræ floating tongue and the triggering of the current retreat, *J. Geophys. Res.*, *116*, F01007, doi:10.1029/2009JF001632.

Münchow, A., K. K. Falkner, and H. Melling (2007), Spatial continuity of measured seawater and tracer fluxes through Nares Strait, a dynamically wide channel bordering the Canadian Archipelago, *J. Mar. Res.*, *65*(6), 759–788.

Münchow, A., K. K. Falkner, and H. Melling (2015), Baffin Island and West Greenland Current Systems in northern Baffin Bay, *Prog. Oceanogr.*, *132*, 305–317.

Nick, F. M., A. Vieli, I. M. Howat, and I. Joughin (2009), Large-scale changes in Greenland outlet glacier dynamics triggered at the terminus, *Nat. Geosci.*, *2*(2), 110–114.

Noël, B., W. J. Van De Berg, E. Van Meijgaard, P. Kuipers Munneke, R. Van De Wal, and M. R. Van Den Broeke (2015), Evaluation of the updated regional climate model RACMO2.3: Summer snowfall impact on the Greenland Ice Sheet, *Cryosphere*, *9*(5), 1831–1844.

O'Callaghan, J. F., and D. M. Mark (1984), The extraction of drainage networks from digital elevation data, *Comput. Vis. Graph. Image Process.*, *28*(3), 323–344.

O'Leary, M., and P. Christoffersen (2013), Calving on tidewater glaciers amplified by submarine frontal melting, *Cryosphere*, *7*(1), 119–128.

Porter, D. F., K. J. Tinto, A. Boghosian, J. R. Cochran, R. E. Bell, S. S. Manizade, and J. G. Sonntag (2014), Bathymetric control of tidewater glacier mass loss in northwest Greenland, *Earth Planet. Sci. Lett.*, *401*, 40–46.

Rignot, E., M. Koppes, and I. Velicogna (2010), Rapid submarine melting of the calving faces of west Greenland glaciers, *Nat. Geosci.*, *3*(3), 187–191.

Rignot, E., I. Fenty, Y. Xu, C. Cai, and C. Kemp (2015), Undercutting of marine-terminating glaciers in west Greenland, *Geophys. Res. Lett.*, *42*, 5909–5917, doi:10.1002/2015GL064236.

Rignot, E., I. Fenty, Y. Xu, C. Cai, I. Velicogna, C. Ó. Cofaigh, and D. Duncan (2016a), Bathymetry data reveal glaciers vulnerable to ice-ocean interaction in Uummannaq and Vaigat glacial fjords, west Greenland, *Geophys. Res. Lett.*, *43*, 2667–2674, doi:10.1002/2016GL067832.

Rignot, E., Y. Xu, D. Menemenlis, J. Mouginot, B. Scheuchl, X. Li, and C. Cai (2016b), Modeling of ocean-induced ice melt rates of five west Greenland glaciers over the past two decades, *Geophys. Res. Lett.*, *43*, 6374–6382, doi:10.1002/2016GL068784.

Sciascia, R., F. Straneo, C. Cenedese, and P. Heimbach (2013), Seasonal variability of submarine melt rate and circulation in an east Greenland fjord, *J. Geophys. Res. Oceans*, *118*, 2492–2506, doi:10.1002/jgrc.20142.

Shepherd, A., E. R. Ivins, A. Geruo, V. R. Barletta, M. J. Bentley, S. Bettadpur, and M. Horwath (2012), A reconciled estimate of ice-sheet mass balance, *Science*, *338*(6111), 1183–1189.

Slater, D. A., P. W. Nienow, T. R. Cowton, D. N. Goldberg, and A. J. Sole (2015), Effect of near-terminus subglacial hydrology on tidewater glacier submarine melt rates, *Geophys. Res. Lett.*, *42*, 2861–2868, doi:10.1002/2014GL062494.

Slater, D. A., D. N. Goldberg, P. W. Nienow, and T. R. Cowton (2016), Scalings for submarine melting at tidewater glaciers from buoyant plume theory, *J. Phys. Oceanogr.*, *46*(6), 1839–1855.

Smith, P. C. (1975), A streamtube model for bottom boundary currents in the ocean, *Deep Sea Res. Oceanogr. Abstr.*, *22*(12), 853–873.

Stevens, L. A., F. Straneo, S. B. Das, A. J. Plueddemann, A. L. Kukulya, and M. Morlighem (2016), Linking glacially modified waters to catchment-scale subglacial discharge using autonomous underwater vehicle observations, *Cryosphere*, *10*(1), 417–432.

Straneo, F., and C. Cenedese (2015), The dynamics of Greenland's glacial fjords and their role in climate, *Annu. Rev. Mar. Sci.*, *7*, 89–112.

Straneo, F., and P. Heimbach (2013), North Atlantic warming and the retreat of Greenland's outlet glaciers, *Nature*, *504*(7478), 36–43.

Straneo, F., G. S. Hamilton, D. A. Sutherland, L. A. Stearns, F. Davidson, M. O. Hammill, and A. Rosing-Asvid (2010), Rapid circulation of warm subtropical waters in a major glacial fjord in east Greenland, *Nat. Geosci.*, *3*(3), 182–186.

Straneo, F., R. G. Curry, D. A. Sutherland, G. S. Hamilton, C. Cenedese, K. Våge, and L. A. Stearns (2011), Impact of fjord dynamics and glacial runoff on the circulation near Helheim glacier, *Nat. Geosci.*, *4*(5), 322–327.

Straneo, F., D. A. Sutherland, D. Holland, C. Gladish, G. S. Hamilton, H. L. Johnson, and M. Koppes (2012), Characteristics of ocean waters reaching Greenland's glaciers, *Ann. Glaciol.*, *53*(60), 202–210.

Sutherland, D. A., and F. Straneo (2012), Estimating ocean heat transports and submarine melt rates in Sermilik fjord, Greenland, using lowered acoustic Doppler current profiler (LADCP) velocity profiles, *Ann. Glaciol.*, *53*(60), 50–58.

Sutherland, D. A., F. Straneo, and R. S. Pickart (2014), Characteristics and dynamics of two major Greenland glacial fjords, *J. Geophys. Res. Oceans*, *119*, 3767–3791, doi:10.1002/2013JC009786.

Tarboton, D. G. (1997), A new method for the determination of flow directions and upslope areas in grid digital elevation models, *Water Resour. Res.*, *33*(2), 309–319, doi:10.1029/96WR03137.

van den Broeke, M., J. Bamber, J. Ettema, E. Rignot, E. Schrama, W. J. van de Berg, and B. Wouters (2009), Partitioning recent Greenland mass loss, *Science*, *326*(5955), 984–986.

Vieli, A., and F. M. Nick (2011), Understanding and modelling rapid dynamic changes of tidewater outlet glaciers: Issues and implications, *Surv. Geophys.*, *32*(4–5), 437–458.

Xu, Y., E. Rignot, D. Menemenlis, and M. Koppes (2012), Numerical experiments on subaqueous melting of Greenland tidewater glaciers in response to ocean warming and enhanced subglacial discharge, *Ann. Glaciol.*, *53*(60), 229–234.

Xu, Y., E. Rignot, I. Fenty, D. Menemenlis, and M. Flexas (2013), Subaqueous melting of Store Glacier, west Greenland from three-dimensional, high-resolution numerical modeling and ocean observations, *Geophys. Res. Lett.*, *40*, 4648–4653, doi:10.1002/grl.50825.